Universität Hamburg

Synchrotron Research Institute

YEREVAN STATE UNIVERSITY

German-Armenian Joint Practical Course
on Accelerator Physics

Electron Beam Parameter Measurements

Supervisor: Dr. Artsrun Sargsyan

Federal Foreign Office

Supported by the German Federal Foreign Office under Kapitel 0504, Titel 68713

YEREVAN, ARMENIA
2019

Contents

1. Introduction

The present chapter 1 provides an overview of various accelerator principles as a background of the essentials of this course. The less interested students may skip this chapter (which would be certainly a pity!) and start with chapter 2 right away.

1.1 Why do we need particle accelerators?

In contemporary scientific research, the structure of various natural and man-made objects, their basic building blocks and the interaction between these blocks and structures are of great interest. Taking an atomic scale motion picture of a chemical process or unraveling the complex molecular structure of a single protein or virus are the new existing experiments. In Fig. 1.1 the characteristic sizes and times for various structures and processes are shown. The structures usually have extraordinarily small sizes, sometimes well below $10^{-15}m$, and the time of some processes about a few femtoseconds (1 fs = 10^{-15} sec).

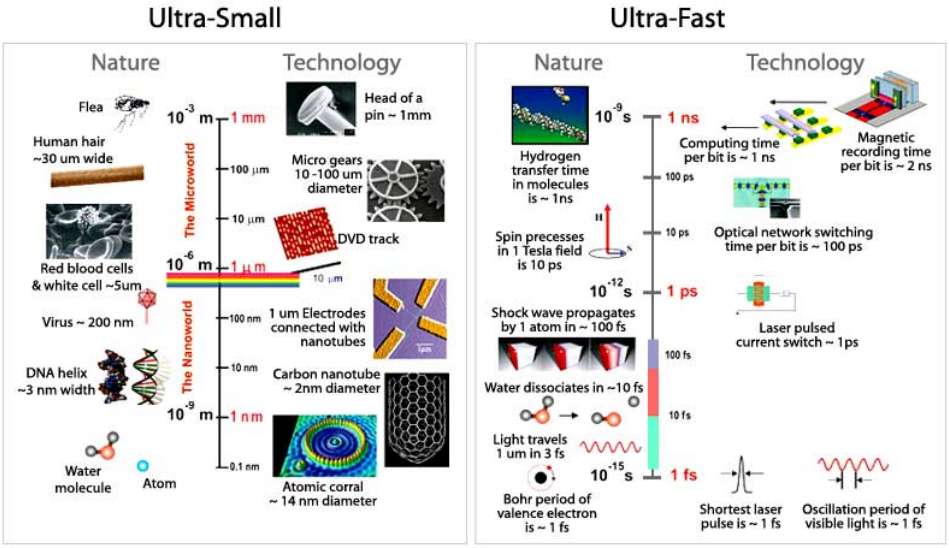

Figure 1.1. The characteristic sizes and times for various structures and processes.

The microblocs/microparticles and ultrafast processes in a matter can be studied by means of ultrashort beams of electromagnetic radiation and/or high energy charged particles. The wavelength of the electromagnetic radiation must be small compared to the size of a structure.

The photon energy E_γ for the wavelength $\lambda = 10^{-15}m$ is

$$E_\gamma = h\nu = \frac{hc}{\lambda} = 2 * 10^{-10}J. \qquad (1.1)$$

Such high energy photon beams are usually generated by accelerated/decelerated charged particles having energy E_e greater than E_γ. The conventional method of obtaining high energy charged particles is based on the interaction with high electric fields. In particular, to obtain electron beams being able to generate photons with energy given in (1.1), they should be passed through the potential difference $U > 1.2 * 10^9 V$ ($E_e = eU$).

If investigations in matter are carried out directly with particle beams, then the length of the particle De Broglie wave should be smaller than the characteristic sizes of the system.

$$\lambda_B = \frac{h}{p} = \frac{hc}{E}, \tag{1.2}$$

where p and E are the momentum and energy of particles.

In the SI system the unit for measuring an energy is J (Joule), but in high energy physics the eV (electron volt) units are more suitable. 1eV is the kinetic energy gained by a particle of elementary charge $e = 1.602 \times 10^{-19} C$ as it crosses a potential difference of $\Delta U = 1V$. The conversion factor thus is $1eV = 1.602 \times 10^{-19} J$.

Another important application of high energy charged particles is the production of new heavy elementary particles via beam-beam collision. The amount of energy needed to produce new particles should be greater than the sum of rest energies of produced particles. Recall that the rest energy of a particle is defined by the fundamental relation

$$E = m_0 c^2, \tag{1.3}$$

where m_0 is the rest mass of the particle.

1.2 Forces to accelerate particles

In the first part it was shown that the high energy particle beams are important tools in nowadays research. Accelerators are the devices which accelerate the charged particle beams. Since the velocity of high energy particles is close to the speed of light ($c = 3 * 10^8 m/s$), the energy must be considered in the relativistic form

$$E = \sqrt{m_0^2 c^4 + p^2 c^2} \tag{1.4}$$

Here m_0 is the rest mass and p is the momentum of the particle. The relativistic particle momentum is given by the relation $p = \gamma m_0 c$, where $\gamma = \sqrt{1-\beta^2}$ is the Lorentz factor and $\beta = \frac{v}{c}$. The only free variable in Eq. (1.4) is the momentum p and, therefore, to increase the energy we should increase the momentum p.

According to the Newton's second law the only way to change the momentum p of the particle is to act by a force F

$$\dot{\boldsymbol{p}} = \boldsymbol{F} \tag{1.5}$$

In order to reach high kinetic energies, sufficiently strong force must be acted on the particle on sufficient period of time.

In nature we have four types of interactions**:** **strong**, **weak**, **gravity** and **electromagnetic**. For **strong** and **weak** forces the action range is below $10^{-15}m$ and therefore these forces are not usable for acceleration of the particles. **Gravity** is many orders of magnitude weaker. The only possible option is to use **electromagnetic** forces. On a charged particle with velocity v and charge q, the electromagnetic field with the magnetic component $\boldsymbol{B}$ and electric component $\boldsymbol{E}$ acts by the Lorentz force

$$F_l = q(\boldsymbol{v} \times \boldsymbol{B} + \boldsymbol{E}) \tag{1.6}$$

As the particle moves from some position $\boldsymbol{r_1}$ to $\boldsymbol{r_2}$, its energy changes by the amount

$$\Delta E = \int_{\boldsymbol{r_1}}^{\boldsymbol{r_2}} \boldsymbol{F} d\boldsymbol{r} = q \int_{\boldsymbol{r_1}}^{\boldsymbol{r_2}} (\boldsymbol{v} \times \boldsymbol{B} + \boldsymbol{E}) d\boldsymbol{r}. \tag{1.7}$$

During the motion the path element $d\boldsymbol{r}$ is always parallel to the velocity vector $\boldsymbol{v}$. The vector $\boldsymbol{v} \times \boldsymbol{B}$ is thus perpendicular to $d\boldsymbol{r}$, i.e. $(\boldsymbol{v} \times \boldsymbol{B}) \cdot \boldsymbol{dr} = \boldsymbol{0}$. Hence the magnetic field $\boldsymbol{B}$ does not change the energy of the particle. An increase in energy can thus only be achieved by the use of electric fields. The gain in energy directly follows by Eq. (1.7) and is

$$\Delta E = \int_{\boldsymbol{r_1}}^{\boldsymbol{r_2}} \boldsymbol{E} d\boldsymbol{r} = eU \tag{1.8}$$

where U is the voltage crossed by the particle.

Although the magnetic field does not contribute to the energy of the particle, it is required to steer, bend and focus charged particle beams.

The main tasks in accelerator physics are the acceleration and steering of charged particle beams. Both processes rely on the interaction with electromagnetic forces and hence on the foundations of the classical electrodynamics. Here Maxwell's equations are of fundamental importance [1].

1.3 Overview of the accelerators development

Since 1920s various machines were built to accelerate the charged particle beams for experimental physics, always with the principal objective of reaching ever higher energies.

The simplest particle accelerators use a constant electric field between to electrodes, produced by a high voltage generator. This principle is illustrated in Fig 1.2. One of the electrodes represents the particle source. In case of electron beams this is a thermionic cathode. Protons as well as light and heavy ions, are extracted from the gas phase by using a further DC or high frequency voltage to ionize a very rarified gas and so produce a plasma inside the particle source. Charged particles are then continuously emitted from the plasma, and are accelerated by the electric field. In the accelerating region there is a relatively good vacuum, in order to avoid collision with residual gas molecules. The particles are thus continuously accelerated without any loss of energy until they reach the second electrode. There they exit the accelerator and usually traverse a further field-free drift region, through which they travel at constant energy until they reach the target. This principle is very widely employed in research and technology. The particle energies which can be reached by this method, however, is very limited. In electrostatic accelerator the maximum achievable energy is directly proportional to the maximum voltage which can be developed, and this gives the energy limit. At higher voltages the field strength closer to electrodes grows so much that ions and electrons produced in this region are accelerated to considerable energies. They collide with residual gas molecules and so produce many more ions, which themselves undergo the same processes. The result is an avalanche of charge carriers causing spark discharge and the break-down of high voltage. This process, called corona formation, limits the maximum achievable energy.

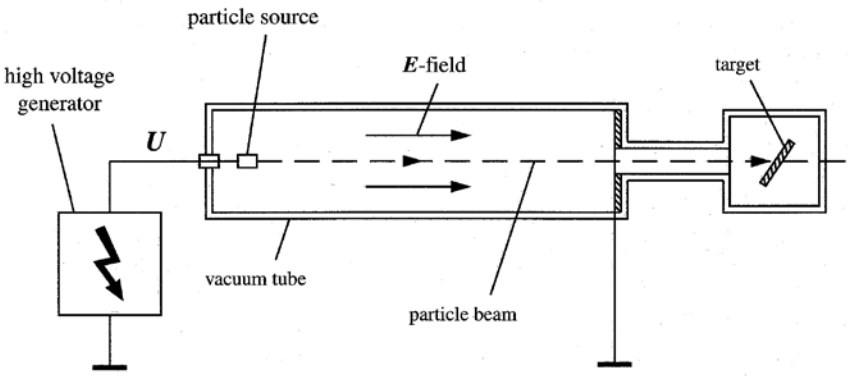

Figure 1.2. General principle of electrostatic accelerator.

In order to avoid this problem the Swede Ising in 1925 suggested to use rapidly changing high frequency voltages instead of direct voltages. Three years later Wideroe performed the first successful test of a linear accelerator based on this principle (Fig. 1.3). It consists of a series of metal drift tubes arranged along the beam axis connected with alternating polarity, to a radiofrequency supply, which delivers a voltage of the form $U(t) = U_{max}Sin(\omega t)$. During a half period the voltage applied to the first drift tube acts to accelerate the particles leaving the ion source. The particles reach the first drift tube with a velocity v_1. They then pass through this drift tube which shields them from external fields. Meanwhile the direction of the RF field is reversed. When they reach the gap between the first and second drift tubes, they again undergo acceleration. This process is repeated for each of the drift tubes. After the i-th drift tube the particles of charge q have reached an energy

$$E_i = iqU_{max}Sin(\Psi_0) \tag{1.9}$$

where Ψ_0 is the average phase of the RF voltage that the particles see as they cross the gaps. It is evident that the energy is again proportional to the number of stages i traversed by the particles. The important point, however, is that the largest voltage in the entire system is never greater then U_{max}. It is therefore possible, in principle, to produce arbitrarily high particle energies without encountering the problem of voltage discharge. This is the decisive advantage of RF accelerators over the electrostatic systems. For this reason almost all particle accelerators nowadays use high-frequency alternating voltages, produced by powerful RF supplies.

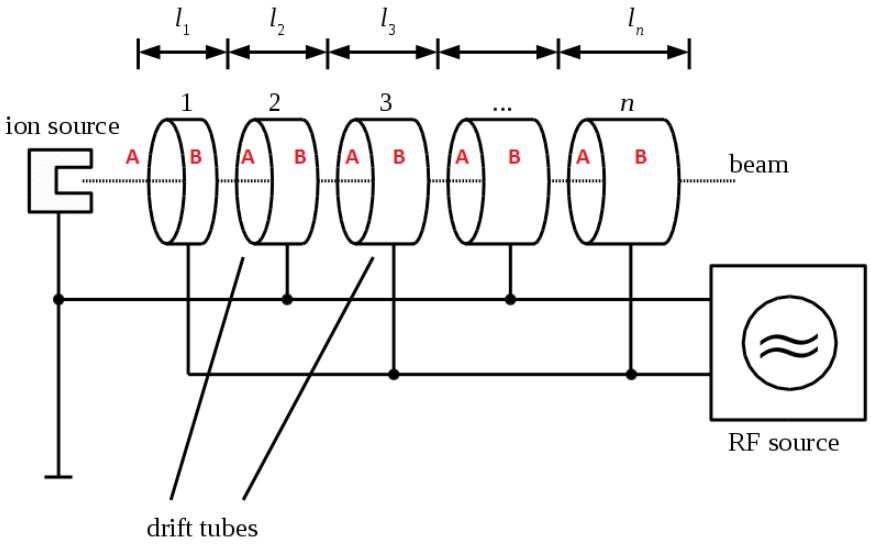

Figure 1.3. Wideroe linear accelerator

Although linear accelerators can in principle reach arbitrarily high particle energies, the length and hence the cost of the machine grows with energy. It is therefore desirable to drive the particles around a circular path and so use the same accelerating structure many times. The first circular accelerator to be developed according to this principle was the cyclotron, proposed by E.O. Lawrence at the University of California in 1930. A year later Livingston succeeded in experimentally demonstrating the operation of such a machine. In 1932 they together built the first proton cyclotron suitable for experiments, with a peak energy of $1.2MeV$.

To make the particles follow a circular path the cyclotron uses an iron magnet which produces a homogeneous magnetic field B_z between its two round poles (Fig. 1.4). The particles circulate in a plane between the poles with a revolution frequency

$$\omega_z = \frac{q}{m} B_z \tag{1.10}$$

which is also known as the cyclotron frequency.

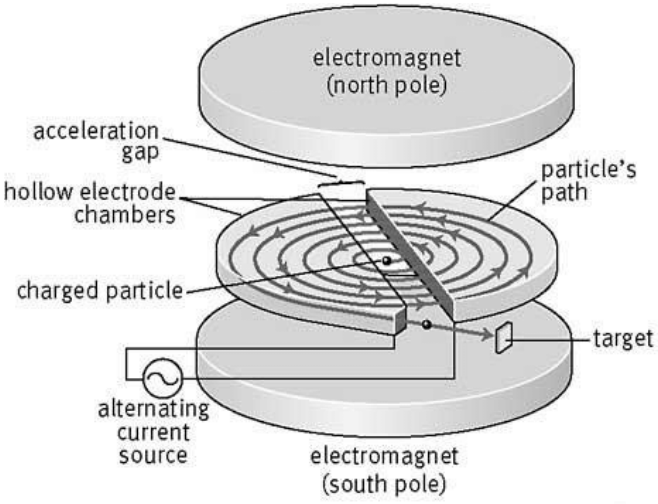

Figure 1.4. The scheme of cyclotron.

Notice that the cyclotron frequency does not depend on the particle velocity at all. This is because of the fact that as the momentum increases, the orbit radius and, hence, the circumference along which the particles travel increase in proportion, provided that the mass m remains constant. This condition is of course only satisfied for non-relativistic particles.

Classical cyclotrons can accelerate protons, deuterons, and alpha particles up to about 22MeV per elementary charge. At these energies the motion is still sufficiently non-relativistic. At higher energies the cyclotron frequency decreases inversely proportional to the increasing particle mass $m(E)$. If the frequency of the RF supply is decreased accordingly, much higher energies can be reached. This principle is employed in the synchrocyclotron.

A more effective method is adopted in the isochroncyclotron, in which the magnetic field is increased in such a way that the cyclotron frequency remains constant, namely

$$\omega_z = \frac{e\, B_z(E)}{m(E)} = Const \tag{1.11}$$

However, this approach is problematic because the beam becomes defocused by the changing magnetic field. To resolve this issue, isochroncyclotrons use magnets with rather complex pole shapes, which compensate this loss of focusing with so-called "edge-focusing". Isochroncyclotrons can reach energies of over $600MeV$.

The principle of the cyclotron, which relies on the revolution frequency being constant, cannot be directly applied on electrons because they quickly reach

relativistic velocities, i.e. $v \approx c$, due to their small rest mass ($m_e = 0.511MeV$). As a result, their mass increases almost proportionally to their energy and the cyclotron frequency decreases in inverse proportion. This effect cannot be counterbalanced by approaches described above.

Strictly speaking it is not actually necessary for the revolution frequency to be constant: it is merely sufficient for the particles to see the same phase of the RF voltage on each revolution. This can be achieved by choosing a relatively high accelerating frequency (typically of around $\nu_{RF} = 3Ghz$) and correspondingly short wavelength. The energy gain per revolution is tuned so that the total circumference of the particle orbit always increases by an exactly integer number of RF wavelength. This principle is employed in the microtron, a type of cyclotron for electrons [1]. The principle of microtron is illustrated in Fig. 1.5.

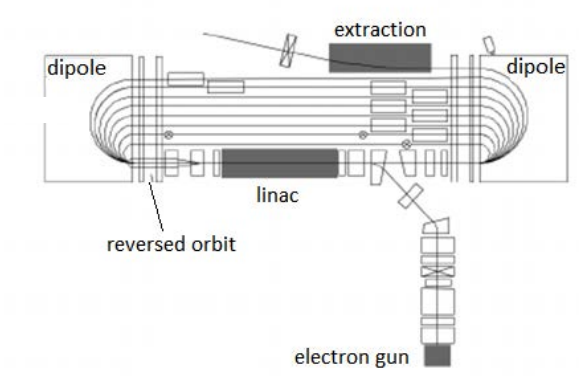

Figure 1.5. The scheme of microtron.

Over the time the achievement of higher beam energies became increasingly important. The relatively compact machines described so far cannot provide such possibilities.

For relativistic particles the orbit radius increases with energy as

$$R = \frac{E}{ecB}. \tag{1.12}$$

There is a technical limit on the magnetic field that can be produced (currently around few Tesla is feasible). This means that at energy $E > 1Gev$ the orbit radius increases to several meters, and it is hardly feasible to produce a magnet having such a size. Instead of using such big magnets, the new concept suggests to use many separate compact bending magnets arranged along a constant beam path. This approach allows handling particle orbits with arbitrary constant radius R. In order to provide a

constant radius, the ratio E/B (see eq. 1.12) must be constant, thus, the magnetic field B must be increased synchronously with the energy E. The brilliant new idea of the synchrotron provides a mechanism by which the particles gain automatically just the proper energy from the accelerating resonator cavities to maintain a constant radius while the magnetic dipole field is increased. This type of accelerator is hence called a synchrotron, see Fig.1.6.

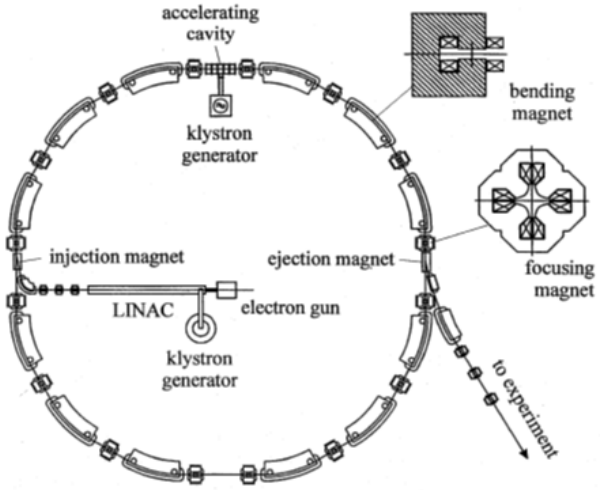

Figure 1.6. Basic layout of modern synchrotron.

The principle of the synchrotron was developed almost simultaneously in 1945 by E.M.McMillan at the University of California and by V. Veksel in the Soviet Union. In that same year construction of the first 320MeV electron synchrotron began at the University of California. A year later, using a very small machine with a maximum energy of 8MeV, F.G.Gourad and D.E. Barnes in England succeeded in confirming the theoretical predictions of the synchrotron functionality. Following these early successes a whole series of synchrotrons were designed and built at the end of the fifties to accelerate protons as well as electrons. Until today the synchrotrons are the powerful experimental tools for science and applications. An intense form of electromagnetic radiation, called synchrotron radiation, is emitted at energies above a few tens of MeV. This type of radiation has very useful properties, and for the past decades has primarily been used in fixed target experiments. The importance of the synchrotron radiation has grown so much around the world that today many machines are built exclusively for this purpose.

More detailed descriptions of above presented accelerators can be found in [1].

2. Linear beam optics

When an accelerator is constructed the desired trajectory of the charged particle beam is fixed. For linear accelerators this trajectory can be a simple straight line. In circular accelerators it may have a very complicated shape. In any kind of accelerators there is exactly one curve on which ideally all particles should move. This curve is called design orbit or ideal orbit. The trajectories of individual particles within a real beam always have a certain angular divergence, and without further measures the particle would eventually hit the wall of the vacuum chamber and be lost. It is therefore necessary, first of all, to fix the particle trajectory, and then repeatedly steer the diverging particles back onto the ideal trajectory. In most general term, this is done by means of electromagnetic field, in which particles of charge q and velocity v experience the Lorentz force (1.6). Magnets are used to steer and focus the beams and electric fields are employed to accelerate them. The physics of beam steering and focusing is called the beam optics [2], considering the analogy with the field studying the light propagation.

2.1 Charged Particle motion in magnetic field

To describe the motion of a particle in the vicinity of the nominal trajectory we introduce a Cartesian coordinate system $K = (x, z, s)$ whose origin moves along the trajectory of the beam (Fig. 2.1). The axis along the beam direction is s, while the horizontal and vertical axes are labeled x and z, respectively.

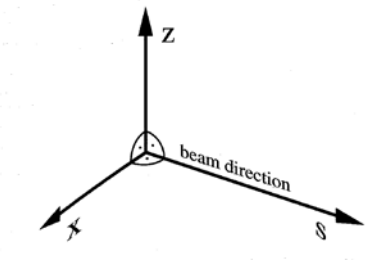

Figure 2.1: Coordinate system to describe the motion of particles.

We will assume that the particles move essentially parallel to the s-direction, i.e. $\boldsymbol{v} = (0,0, v_s)$, and that the magnetic field only has transverse components and so has the form $\boldsymbol{B} = (B_x, B_z, 0)$. For a particle moving in the horizontal plane through the magnetic field there is then a balance between the Lorentz force $F_x = -ev_sB_z$ and the centrifugal force $F_r = mv_s^2/R$. Here m is the mass of a particle and R is the radius of curvature of the trajectory. This balance of forces leads to the relation

$$\frac{1}{R} = \frac{e}{p} B_z(x, z, s) \tag{2.1}$$

if one considers $p = mv_s$. The corresponding expression holds for the vertical direction as well.

Since the transverse dimensions of the beam are small compared to the radius of curvature of the particle trajectory, we may expand the magnetic field in the vicinity of the nominal trajectory (i.e. the design orbit):

$$B_z(x) = B_{z0} + \frac{dB_z}{dx}\, x + \frac{1}{2!}\frac{d^2B_z}{dx^2}x^2 + \frac{1}{3!}\frac{d^3B_z}{dx^3}x^3 + \cdots \tag{2.2}$$

Multiplying by e/p one obtains

$$\begin{gathered}\frac{e}{p}B_z(x) = \frac{e}{p}B_{z0} + \frac{e}{p}\frac{dB_z}{dx}\, x + \frac{e}{p}\frac{1}{2!}\frac{d^2B_z}{dx^2}x^2 + \frac{e}{p}\frac{1}{3!}\frac{d^3B_z}{dx^3}x^3 + \cdots = \\ \frac{1}{R} \quad + \quad kx \quad + \quad \frac{1}{2!}mx^2 \quad + \quad \frac{1}{3!}0x^3 + \cdots \\ \text{dipole} \qquad \text{quadrupole} \qquad \text{sextupole} \qquad \text{octupole}\end{gathered} \tag{2.3}$$

The magnetic field around the beam may therefore be regarded as a sum of multipoles, each of which has a different effect on the path of the particle. The first term describes a dipole field which serves for beam deflection. The second term corresponds to a quadrupole with field strength k. It serves for beam focusing. If only the two lowest multipoles are used for the beam steering in an accelerator then one speaks of linear beam optics, since only constant and linearly distracting forces act.

2.2 Accelerator magnets

Conventional iron magnets consist of current-carrying conductors and iron poles, which amplify the field. For a static magnetic field in vacuum, the Maxwell equations apply

$$\boldsymbol{\nabla} \times \boldsymbol{H} = 0 \quad \boldsymbol{\nabla H} = 0 \tag{2.4}$$

In this case the magnetic field can be written in terms of a scalar potential $\varphi(x, z, s)$ which defines the field uniquely:

$$\boldsymbol{H} = \nabla\varphi. \tag{2.5}$$

It is more convenient to use the magnetic flux density $\boldsymbol{B} = \mu_r \mu_0 \boldsymbol{H}$, where μ_r is the magnetic permeability of pole material. Introducing a potential $\Phi(x, z, s) = \mu_r \mu_0 \varphi(x, z, s)$, the magnetic flux density may be calculated according to

$$B = \nabla \Phi \,. \tag{2.6}$$

From the Maxwell's equations it follows that the potential Φ satisfies the Laplace equation:

$$\nabla^2 \Phi = 0. \tag{2.7}$$

Equations (2.6) and (2.7) form the theoretical basis for the design of conventional magnets. The potential Φ can be used to determine the form of the iron poles which can generate the desired magnetic field distribution.

2.2.1. Dipole magnet

Dipole magnets are used to bend charged particles onto a circular path. They provide a constant field along the both x and s axes

$$B_z(x, s) = const \tag{2.8}$$

The required potential then can be found immediately from (2.6)

$$\Phi(x, z, s) = B_0 \, z \tag{2.9}$$

The equipotential surfaces $\Phi(x, z, s) = \Phi_0 = const$ are therefore surfaces parallel to the x, s plane. The dipole consists of two parallel iron poles of separation $h = 2z_0$ (Fig.2.2).

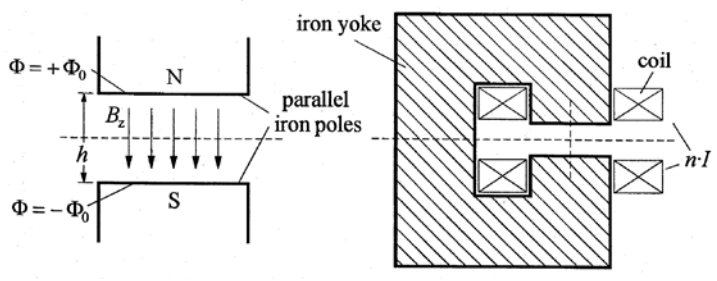

Figure 2.2: The magnetic field of an ideal dipole magnet of two parallel iron poles (left). The schematic structure of a dipole magnet and the integration path for the calculation of the magnetic field (right).

The magnetic field $\boldsymbol{B}$ between the iron poles depends on the current I which is flowing through the coils. This relationship may be calculated most simply by using the Ampere's law.

$$\oint \boldsymbol{H}\, ds = I_{tot} = nI, \tag{2.10}$$

where n is the number of windings of the coil. For simplicity we assume that the field H_0 in the gap and H_{Fe} in the iron is always constant. If now we notice that $H_{Fe} = H_0/\mu_r$ with $\mu_r \gg 1$, and take the path of integration as illustrated in fig. 2.2, we obtain

$$nI = \oint \boldsymbol{H} ds = H_{Fe} l_{Fe} + H_0 h \approx H_0 h \tag{2.11}$$

The magnetic field in the gap is $B_0 = \mu_0 H_0$ since $\mu_r = 1$ there. We thus obtain the following expression for the field of a dipole magnet:

$$B_0 = \mu_0 \frac{nI}{h} \tag{2.12}$$

The dipole strength in (2.3) is then

$$\frac{1}{R} = \frac{e}{p} B_0 = \frac{e\mu_0}{p} \frac{nI}{h} \tag{2.13}$$

The result which we derived here is idealized. A magnetic field is homogeneous only for infinitely wide poles and the relation between the magnetic field and the current is linear only at low field strengths, i.e. $B < 1T$. The iron turns into saturation above $1T$.

2.2.2. Quadrupole magnet

To focus the beams, quadruple fields are used which, according to (2.3), disappear along the beam axis and increase linearly with transverse distance x. Their field shape may then be determined from the function

$$B_z(x) = gx \text{ with } g = \frac{\partial B_z}{\partial x} \tag{2.14}$$

The second derivation of B_z also disappears in this case. Because of $\boldsymbol{\nabla} \times \boldsymbol{B} = 0$, such a field must also have a horizontal component. The required potential is then

$$\Phi(x, z) = gxz. \tag{2.15}$$

The effect of the quadrupole magnet on the beam is determined by the quadrupole strength

$$k = \frac{eg}{p}\,. \tag{2.16}$$

which has the unit $1/m^2$. The equipotential lines $z(x)$ for a given value of Φ_0 are hyperbolae of the form

$$z(x) = \frac{\Phi_0}{gx} \tag{2.17}$$

Therefore, a quadrupole consists of four poles with hyperbolic surfaces, arranged with alternating polarity N-S-N-S, as shown in Fig. 2.3. The four poles are excited by coils which surround them. The distribution of field lines between the poles makes a magnet which focuses the beam in the horizontal direction and defocuses in the vertical direction. To properly focus the beam it therefore is necessary to use at least two quadrupoles, rotated through 90° relative to each other.

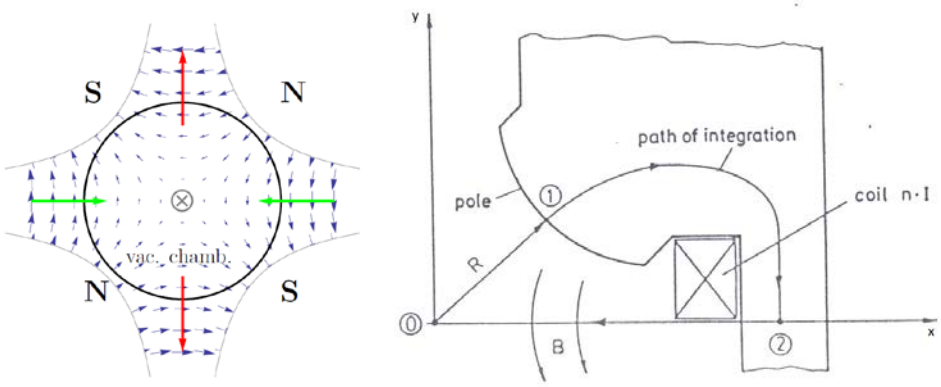

Figure 2.3. The magnetic field of a horizontally focusing Quadrupole magnets (left). A schematic cross section through a quadrupole magnet with the integration path (right). Note: The coordinate y in this picture corresponds to z in our previous equations.

The relationship between the current I in the coils and the field strenght may easly be determined again using Ampere laws. Choosing an inegration path which begins on the beam axis (point 0) and runs through the saddle point of the pole (point 1), through the iron yoke to the x-axis(point 2), and from there back to the starting point 0.

The integral may then be broken up into pieces as follows:

$$\oint \boldsymbol{H} d\boldsymbol{s} = \int_0^1 \boldsymbol{H}_0 d\boldsymbol{s} + \int_0^2 \boldsymbol{H}_{Fe} d\boldsymbol{s} + \int_2^0 \boldsymbol{H} d\boldsymbol{s} = nI \qquad (2.18)$$

The only non-zero contribution to the right hand side of the equation comes from the integration from the beam axis to the pole ($0 \rightarrow 1$). Within the iron yoke the integral vanishes because $\mu_r \gg 1$ means that H_{Fe} is negligible. The integral along the x-axis is also zero, because here we always have $H \perp \boldsymbol{s}$. We therefore only need to consider the field between the beam axis and the pole. This field may be obtained immediately from the expression for the potential (2.15) and is given by $B_x = gz$ and $B_z = gx$. The contribution of the magnetic field along the path of integration $0 \rightarrow 1$ is then given by

$$H = \frac{g}{\mu_0}\sqrt{x^2 + z^2} = \frac{g}{\mu_0}\sqrt{2}x = \frac{g}{\mu_0}r \tag{2.19}$$

Here we consider $x = z$ for this particular choice of path of integration and so r gives the line of integration from the origin. The apex of the pole is at $r = a$, allowing the integral (2.18) to be written as

$$\int_0^a H dr = \frac{g}{\mu_0}\int_0^a r dr = \frac{g}{\mu_0}\frac{a^2}{2} = nI \tag{2.20}$$

From here it immediately follows that

$$g = \frac{2\mu_0 nI}{a^2} \tag{2.21}$$

Since $g \sim 1/a^2$ it makes sense to keep the pole separation a as small as possible for high-strength quadrupoles, so that the current I and hence the power consumption of the magnet are reduced.

2.2.3 Solenoid magnet

Another focusing magnet is the solenoid magnet, which consists of a rotationally symmetric coil, see Fig. 2.4. On the basis of Maxwell's equation $\boldsymbol{divB} = 0$, the magnetic field, which is purely longitudinal in the inner part of the coil, must contain radial components in the outer part. While particles moving exactly on axis do not experience any force, the others get an azimuthal acceleration while entering and leaving the magnets because of radial components. Due to the azimuthal motion there is a radial force in the longitudinal field. This force is proportional to the radial distance r and therefore can be used for focusing. The focal length f_{sol} is given by

$$\frac{1}{f_{sol}} = \int \left(\frac{eB_s}{2p}\right)^2 ds \tag{2.22}$$

As seen from eq. (2.22) f_{sol} increases with the square of the particle's momentum p. Therefore a solenoid lens is effective only for small momenta. At $p \gg 1 MeV/c$, a quadrupole magnet is much more effective.

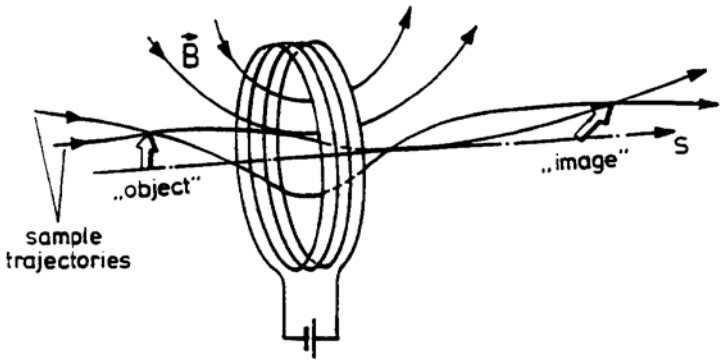

Figure 2.4: Scheme of a solenoid magnet with field lines and particle trajectories.

2.3 Transformation Matrices

To determine the motion of particles, first we write the general equation of motion in the moving coordinate system $K = (x, z, s)$ (Fig. 2.1). In general the bending strength $1/\rho$ and the focusing strength k are functions of the path length s along the reference orbit. The linear equation of motion for the particles are [2]

$$\begin{aligned} x''(s) + \left(\frac{1}{\rho^2(s)} - k(s)\right)x(s) &= \frac{1}{\rho}\frac{\Delta p}{p} \\ z''(s) + k(s)z(s) &= 0 \end{aligned} \tag{2.23}$$

where p is the nominal momentum of the particles and Δp is the momentum deviation. The general solution $x(s)$ is the sum of the general solution x_h of the homogeneous equation and a particular solution x_i of the inhomogeneous equation

$$x(s) = x_h(s) + x_i(s) \tag{2.24}$$

With

$$\begin{aligned} x_h''(s) + \left(\frac{1}{\rho^2(s)} - k(s)\right)x_h(s) &= 0 \\ x_i''(s) + \left(\frac{1}{\rho^2(s)} - k(s)\right)x_i(s) &= \frac{1}{\rho}\frac{\Delta p}{p} \end{aligned} \tag{2.25}$$

Since $\Delta p/p$ is assumed to be constant it is obvious that if x_i is a solution for a given $\Delta p/p$, $n \cdot x_i$ will be a solution for $n \cdot \Delta p/p$. Therefore it is useful to normalize x_i with respect to $\Delta p/p$:

$$D(s) = \frac{x_i}{\frac{\Delta p}{p}} \tag{2.26}$$

$D(s)$ is the dispersion trajectory, defined as a particular solution of the following inhomogeneous equation

$$D''(s) + \left(\frac{1}{\rho^2(s)} - k(s)\right) D(s) = \frac{1}{\rho(s)} \tag{2.27}$$

It describes the momentum-dependent part of the motion. The general solution of (2.23) now reads as

$$\begin{aligned} x(s) &= C(s)x_0 + S(s)x_0' + D(s)\frac{\Delta p}{p} \\ z(s) &= C(s)z_0 + S(s)z_0' \end{aligned} \tag{2.28}$$

Here x_0 and z_0 are the initial values of the horizontal and vertical displacements, x_0' and z_0' the initial values of the horizontal and vertical slopes from the nominal trajectory. Here $D_0 = D_0' = 0$ are considered as initial conditions. $C(s)$ and $S(s)$ are two independent solutions of the homogeneous equation:

$$\begin{aligned} C''(s) + \left(\frac{1}{\rho^2(s)} - k(s)\right) C(s) = 0, \\ S''(s) + \left(\frac{1}{\rho^2(s)} - k(s)\right) S(s) = 0. \end{aligned} \tag{2.29}$$

The solutions which satisfy the initial conditions $C_0 = 1, C_0' = 0, S_0 = 0, S_0' = 1,$ are called “Cosinelike” and “Sinelike” trajectories.

The particle coordinates are related to their initial values by a linear transformation, which can also be described by transfer matrices

$$\begin{aligned} \begin{pmatrix} x \\ x' \\ \Delta p/p \end{pmatrix}_s &= \begin{pmatrix} C & S & D_x \\ C' & S' & D_x' \\ 0 & 0 & 1 \end{pmatrix} \begin{pmatrix} x \\ x' \\ \Delta p/p \end{pmatrix}_0, \\ \begin{pmatrix} z \\ z' \\ \Delta p/p \end{pmatrix}_s &= \begin{pmatrix} C & S & 0 \\ C' & S' & 0 \\ 0 & 0 & 1 \end{pmatrix} \begin{pmatrix} z \\ z' \\ \frac{\Delta p}{p} \end{pmatrix}_0. \end{aligned} \tag{2.30}$$

The matrix notation of the solution of the equations of motion is particularly useful if the bending strength $1/\rho(s)$ and the focusing strength $k(s)$ are constant, because in this case the matrix elements can be expressed analytically. The solution for the complete magnetic system is then the product of the individual matrices in the desired sequence. The transfer matrices of the most important magnets are

discussed in the following. They may be used as building blocks to assemble the complete magnetic lattice. To simplify the derivations, it is assumed that the magnetic fields at the input and output of the components have a step function form (hard edge approximation).

2.3.1. Drift space

In a drift space, no external force acts on the particles. The transformation matrix depends only on the length L of the drift space.

$$\frac{1}{\rho(s)} = 0 \text{ and } k(s) = 0 \;\rightarrow\; M_x = M_z = \begin{pmatrix} 1 & L & 0 \\ 0 & 1 & 0 \\ 0 & 0 & 1 \end{pmatrix} \tag{2.31}$$

2.3.2. Dipole sector magnet

A dipole magnet whose edges are perpendicular to the ideal orbit is called sector magnet (Figure 2.5). This magnet acts only on the horizontal direction. In the vertical direction the particle trajectory is like in the drift space

$$k(s) = 0 \text{ and } \varphi = \frac{l}{\rho} \rightarrow M_x = \begin{pmatrix} Cos\varphi & \rho Sin\varphi & \rho(1 - Cos\varphi) \\ -\frac{1}{\rho} Sin\varphi & Cos\varphi & Sin\varphi \\ 0 & 0 & 1 \end{pmatrix}, M_z = \begin{pmatrix} 1 & l & 0 \\ 0 & 1 & 0 \\ 0 & 0 & 1 \end{pmatrix} \tag{2.32}$$

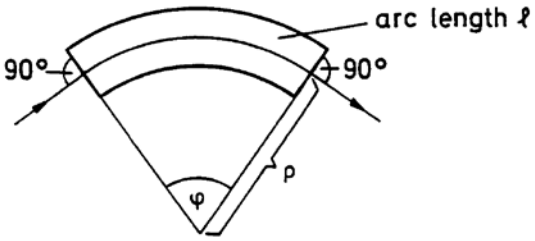

Figure 2.5 Sector dipole magnet.

2.3.3. Quadrupole magnet

For the quadrupole magnet we have $\frac{1}{\rho(s)} = 0$. If $k > 0$,

$$M_x = \begin{pmatrix} Cosh\varphi & \frac{1}{\sqrt{|k|}} Sinh\varphi & 0 \\ \sqrt{|k|}\, Sinh\varphi & Cosh\varphi & 0 \\ 0 & 0 & 1 \end{pmatrix} \tag{2.33}$$

$$M_z = \begin{pmatrix} Cos\varphi & \frac{1}{\sqrt{|k|}}Sin\varphi & 0 \\ -\sqrt{|k|}\,Sin\varphi & Cos\varphi & 0 \\ 0 & 0 & 1 \end{pmatrix},$$

where $\varphi = l\sqrt{|k|}$. These matrices describe horizontal defocusing and vertical focusing. For the case $k < 0$ the matrices M_x and M_z are interchanged and we get horizontal focusing and vertical defocusing.

In many practical cases, the focal length f of the quadrupole magnet is much longer than the length of the lens:

$$f = \frac{1}{kl} \gg l \tag{2.34}$$

In these cases the transfer matrices can be approximated by

$$\begin{aligned} M_x &= \begin{pmatrix} 1 & 0 & 0 \\ \frac{1}{f} & 1 & 0 \\ 0 & 0 & 1 \end{pmatrix} \\ M_z &= \begin{pmatrix} 1 & 0 & 0 \\ -\frac{1}{f} & 1 & 0 \\ 0 & 0 & 1 \end{pmatrix} \end{aligned} \tag{2.35}$$

Note that these matrices describe a lens of zero length, i.e. they are derived from Eq. (2.33) using $l \to 0$ while keeping $k \cdot l = const$. The true length l of the lens has to be recovered by two drift spaces $l/2$ on either side, e.g.

$$\begin{aligned} M_x &= \begin{pmatrix} 1 & \frac{l}{2} & 0 \\ 0 & 1 & 0 \\ 0 & 0 & 1 \end{pmatrix} \begin{pmatrix} 1 & 0 & 0 \\ \frac{1}{f} & 1 & 0 \\ 0 & 0 & 1 \end{pmatrix} \begin{pmatrix} 1 & \frac{l}{2} & 0 \\ 0 & 1 & 0 \\ 0 & 0 & 1 \end{pmatrix} = \begin{pmatrix} 1+\frac{l}{2f} & l+\frac{l^2}{4f} & 0 \\ \frac{1}{f} & 1+\frac{l}{2f} & 0 \\ 0 & 0 & 1 \end{pmatrix} \\ M_z &= \begin{pmatrix} 1 & \frac{l}{2} & 0 \\ 0 & 1 & 0 \\ 0 & 0 & 1 \end{pmatrix} \begin{pmatrix} 1 & 0 & 0 \\ -\frac{1}{f} & 1 & 0 \\ 0 & 0 & 1 \end{pmatrix} \begin{pmatrix} 1 & \frac{l}{2} & 0 \\ 0 & 1 & 0 \\ 0 & 0 & 1 \end{pmatrix} = \begin{pmatrix} 1-\frac{l}{2f} & l-\frac{l^2}{4f} & 0 \\ -\frac{1}{f} & 1-\frac{l}{2f} & 0 \\ 0 & 0 & 1 \end{pmatrix} \end{aligned} \tag{2.36}$$

2.3.4. Solenoid magnet

The transfer matrices of solenoid magnets can't be divided into vertical and horizontal sub matrices, because of the coupling between particle motions in two transverse planes. For the short solenoid magnet the transformation matrix for the 4D vector $(x;\ x';\ z;\ z')$ is presented. The short lens approximation is done as in case of quadrupoles. For that purpose, the transfer matrix M of the whole solenoid is presented as the product of three different matrices M_1, M_2, M_3 corresponding to the entrance fringe field, the constant axial magnetic field, and the output fringe field, respectively.

The radial component of the magnetic field induces an angular kick which changes the divergence of the beam. Assuming the kick is localized at a given longitudinal position at the entrance of the solenoid, the matrix M_1 is [3]

$$M_1 = \begin{pmatrix} 1 & 0 & 0 & 0 \\ 0 & 1 & \frac{eB}{2P} & 0 \\ 0 & 0 & 1 & 0 \\ -\frac{eB}{2P} & 0 & 0 & 1 \end{pmatrix} \tag{2.37}$$

with the approximation $P_s \cong P$. At the output of the solenoid, the matrix has the same form with an opposite sign in the kick:

$$M_3 = \begin{pmatrix} 1 & 0 & 0 & 0 \\ 0 & 1 & -\frac{eB}{2P} & 0 \\ 0 & 0 & 1 & 0 \\ \frac{eB}{2P} & 0 & 0 & 1 \end{pmatrix}. \tag{2.38}$$

The transfer matrix for the part inside of the solenoid magnet is given by:

$$M_2 = \begin{pmatrix} 1 & \frac{P}{eB}Sin\theta & 0 & \frac{P}{eB}(1 - Cos\theta) \\ 0 & Cos\theta & 0 & Sin\theta \\ 0 & -\frac{P}{eB}(1 - Cos\theta) & 1 & \frac{P}{eB}Sin\theta \\ -Sin\theta & 0 & 0 & Cos\theta \end{pmatrix} \tag{2.39}$$

For the whole solenoid the product of the three matrices, $M = M_3 \cdot M_2 \cdot M_1$ gives the final transformation matrix:

$$M_2 = \begin{pmatrix} C^2 & CS/\alpha & CS & S^2/\alpha \\ -CS\alpha & C^2 & -S^2\alpha & CS \\ -CS & -S^2\alpha & C^2 & CS/\alpha \\ S^2\alpha & -CS & -CS\alpha & C^2 \end{pmatrix} \tag{2.40}$$

with $S = Sin(\theta/2)$, $C = Cos(\theta/2)$, $\alpha = \frac{eB}{2P}$ and $\theta = 2L\alpha$ where L is the total length of the solenoid. The thin lens approximation is done by assuming that the length $L$is small compared to $1/\alpha$. By keeping the first terms of Taylor expansions for $Cos\theta$ and $Sin\theta$, the matrix is simplified and takes the form:

$$M = \begin{pmatrix} 1 & 0 & 0 & 0 \\ -\frac{1}{f} & 1 & 0 & 0 \\ 0 & 0 & 1 & 0 \\ 0 & 0 & -\frac{1}{f} & 1 \end{pmatrix}, \tag{2.41}$$

where f is the focal length given by: $\frac{1}{f} = \left(\frac{eB}{2P}\right)^2 L$.

3. Phase Space ellipse, emittance and Twiss parameters

The matrix formalism presented above allows us to calculate individual particle trajectories through an arbitrary magnetic system (lattice), taking into account variations (first order) in particle momentum. However, it does not yield any information about the properties of the particle ensemble/beam. Since this is ultimately a decisive factor in the development of the magnetic guide system, we must extend our techniques to describe the behavior of a particle beam. To do this let us consider the equation of motion for a particle with nominal energy ($\Delta p/p = 0$) [2]:

$$y''(s) + K(s)y(s) = 0 \begin{cases} K = k \ for \ y = z \\ K = -k + \frac{1}{\rho^2} \ for \ y = x \end{cases} \tag{3.1}$$

where $K(s)$ is a function of position s.

The trajectory function $y(s)$ describes a transverse oscillation around the design orbit, known as a betatron oscillation, whose amplitude and phase depend on the position s along the orbit.

The general solution of the equation (3.1) and its derivative are [2]

$$y(s) = A\sqrt{\beta(s)}Cos(\Psi(s) + \phi), \tag{3.2}$$

$$y'(s) = -\frac{A}{\sqrt{\beta(s)}}[\alpha(s)Cos(\Psi(s) + \phi) + Sin(\Psi(s) + \phi)], \tag{3.3}$$

where $\beta(s)$ represents the **beta function,** $\alpha(s) = \frac{1}{2}\beta'(s)$ and A is the constant of integration which is defined by the initial conditions and remains constant throughout

the whole beam transport system. Thus, within a magnetic structure the particles perform betatron oscillations with a position-dependent amplitude given by

$$E(s) = A\sqrt{\beta(s)} \tag{3.4}$$

called the beam envelope. Since all particle trajectories lie inside the envelope $E(s)$, it defines the transverse size of the beam (fig. 3.1).

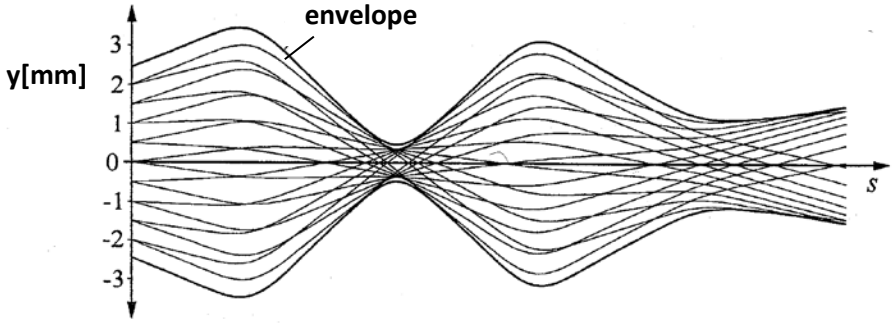

Figure 3.1. Particle trajectories $y(s)$ within the envelope $E(s)$ of the beam.

The beta function $\beta(s)$ is a measure of the beam cross-section. It is defined by the magnetic lattice and varies with the position.

In order to arrive at an expression describing the particle motion in the $y - y'$ phase space we must eliminate the terms which depend on the phase Ψ. From (3.2) and (3.3) we immediately obtain

$$Cos(\Psi(s) + \phi) = \frac{y}{A\sqrt{\beta(s)}}\,, \tag{3.5}$$

$$Sin(\Psi(s) + \phi) = \frac{\sqrt{\beta(s)}y'}{A} + \frac{\alpha(s)y}{A\sqrt{\beta(s)}}\,. \tag{3.6}$$

If we now use the relation $Sin^2\Theta + Cos^2\Theta = 1$ we obtain

$$\frac{y^2}{\beta(s)} + \left(\frac{\alpha(s)}{\sqrt{\beta(s)}} + \sqrt{\beta(s)}y'\right)^2 = A^2\,. \tag{3.7}$$

With the definition

$$\gamma(s) = \frac{1+\alpha^2(s)}{\beta(s)} \tag{3.8}$$

the eq. (3.7) transformes into

$$\gamma(s)y^2(s) + 2\alpha(s)y(s)y'(s) + \beta(s)y'^2(s) = A^2\,. \tag{3.9}$$

This is the general equation of an ellips in the $y - y'$ plane (Fig. 3.2). The area of the phase space ellipse is an important quantity. It is given by πA^2.

Let us now consider a particle beam filling the phase space up to the ellipse with amplitude A_{max}. According to Louville's fundamental theorem [2] the phase space density of particles in the vicinity of any phase space trajectory is invariant if the particles obey the canonical equations of motion. This condition is generally satisfied in accelertors under the condition that the partice energy remains constant and the stochastic effects like beam-gas scattering or synchrotron radiation are negligible. This means that the area of the enclosing phase ellipse is an invariant of the beam motion. As the particles move along the orbit the shape and position of individual ellipses as well as of the enclosing ellipse change according to the amplitude function $\beta(s)$, but areas remain constant. This result has important consequences for the calculation of linear beam optics. The area of the enclosing ellipse of the beam is denoted by $\pi\varepsilon$, where ε is called the beam **emittance.**

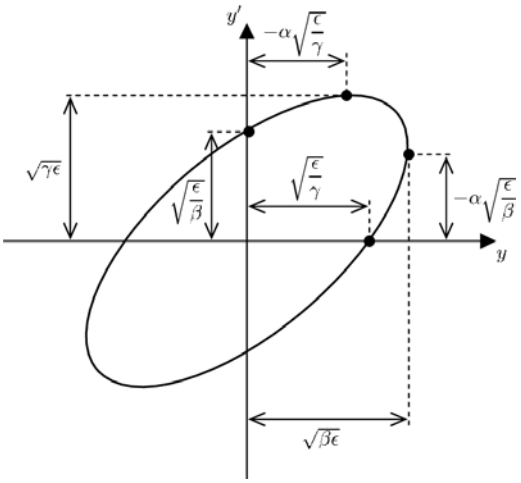

Figure 3.2. The phase space ellipse in the horizontal plane.

When the particles are accelerated, the emittance decreases inversely proportional to the momentum. This can be understood intuitively from the observation that only the longitudinal component of the momentum vector is increased in the accelerating section whereas the transverse components remain invariant, so that the beam divergence shrinks. Therefore we also define the normalized emittance ε_n which remains constant during acceleration.

$$\varepsilon_n = \gamma\beta\varepsilon \tag{3.10}$$

where γ is the Lorentz factor, and $\beta = v/c$.

3.1. Transformation of the beta function

The orientation of the phase ellipse at a point s is characterized by the Twiss parameters $\alpha(s), \beta(s), \gamma(s)$ and the area is determined by the emitance ε.

It is important to know the beam envelope and divergence at each point of the accelerator. Therefore, it is of great interest to know how α, β, γ are transformed through the magnetic system.

We evaluate the invariant A for a single particle at a reference point s_0 and an arbitrary other point s.

$$A^2 = \gamma y^2 + 2\alpha y y' + \beta y'^2 = \gamma_0 y_0^2 + 2\alpha_0 y_0 y_0' + \beta_0 y_0'^2 \tag{3.11}$$

Using the principal trajectories we can relate $y(s), y'(s)$ to $y_0 = y(s_0), y_0' = y'(s_0)$

$$\begin{pmatrix} y \\ y' \end{pmatrix} = \begin{pmatrix} C & S \\ C' & S' \end{pmatrix} \begin{pmatrix} y_0 \\ y_0' \end{pmatrix} \tag{3.12}$$

The inverse transformation matrix is $\begin{pmatrix} S' & -S \\ -C' & C \end{pmatrix}$ so

$$y_0 = S'y - Sy' \tag{3.13}$$

$$y_0' = -C'y + Cy' \tag{3.14}$$

$$A^2 = \gamma_0(S'y - Sy')^2 + 2\alpha_0(S'y - Sy')(-C'y + Cy') + \beta_0(-C'y + Cy')^2 =$$

$$= \gamma y^2 + 2\alpha y y' + \beta y'^2 \tag{3.15}$$

Comparing the coefficients yields:

$$\beta(s) = C^2\beta_0 - 2SC\alpha_0 + S^2\gamma_0 \tag{3.16}$$

$$\alpha(s) = -CC'\beta_0 + (SC' + S'C)\alpha_0 - SS'\gamma_0 \tag{3.17}$$

$$\gamma(s) = C'^2\beta_0 - 2S'C'\alpha_0 + S'^2\gamma_0 \tag{3.18}$$

In matrix notation

$$\begin{pmatrix} \beta \\ \alpha \\ \gamma \end{pmatrix} = \begin{pmatrix} C^2 & -2SC & S^2 \\ -CC' & SC' + S'C & -SS' \\ C'^2 & -2S'C' & S'^2 \end{pmatrix} \begin{pmatrix} \beta_0 \\ \alpha_0 \\ \gamma_0 \end{pmatrix} \tag{3.19}$$

By means of this matrix equation one can transform the beta function piece-wisely through the magnets and drift spaces.

3.2. The Beam matrix

The transverse emittance for a well-centered and aligned beam ($\langle x\rangle, \langle z\rangle, \langle x'\rangle, \langle z'\rangle = 0$) can be determined as [4]

$$\varepsilon_x = \sqrt{det\sigma_x}\ ,\ \varepsilon_z = \sqrt{det\sigma_z}\ , \tag{3.20}$$

where

$$\begin{aligned} \boldsymbol{\sigma}_x &= \begin{pmatrix} \sigma_{11}^{x} & \sigma_{12}^{x} \\ \sigma_{21}^{x} & \sigma_{22}^{x} \end{pmatrix} = \begin{pmatrix} < x^2 > & < xx' > \\ < xx' > & < x'^2 > \end{pmatrix} \\ \boldsymbol{\sigma}_z &= \begin{pmatrix} \sigma_{11}^{z} & \sigma_{12}^{z} \\ \sigma_{21}^{z} & \sigma_{22}^{z} \end{pmatrix} = \begin{pmatrix} < z^2 > & < zz' > \\ < zz' > & < z'^2 > \end{pmatrix} \end{aligned} \tag{3.21}$$

Fig. 3.3 shows the beam ellipse in the $x - x'$ plane, where its tilt angle and dimensions are expressed by means of the elements of the beam matrix.

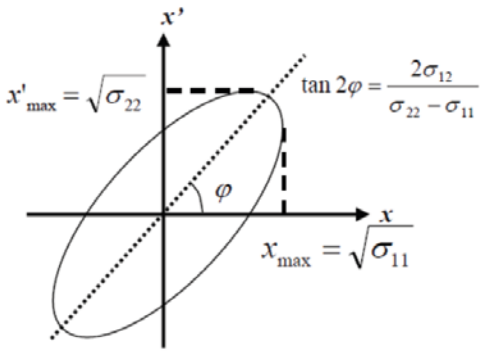

Figure 3.3. Beam ellipse.

The matrix element σ_{11} is the square of the standard deviation of the transverse beam distribution

$$\Sigma_{x,z} = \sqrt{\sigma_{11}^{x,z}}$$

The equation of the phase space ellipse can be written in a different way by using symmetric two dimensional beam matrices

$$(x, x')\sigma_x^{-1}\begin{pmatrix} x \\ x' \end{pmatrix} = 1 \tag{3.23}$$

$$(z, z')\sigma_y^{-1}\begin{pmatrix} z \\ z' \end{pmatrix} = 1 \tag{3.24}$$

Since $\sigma_{12} = \sigma_{21}$ this can be written by

$$\sigma_{22}x^2 - 2\sigma_{21}xx' + \sigma_{11}x'^2 = det\boldsymbol{\sigma}_x = \varepsilon_x^2$$

(with Eq. (3.20)) (3.25)

Comparison with Eq. (3.11) yields the following relations between the Twiss parameters, the emittance, and the beam matrix:

$$\boldsymbol{\sigma}_x = \begin{pmatrix} \sigma_{11}^x & \sigma_{12}^x \\ \sigma_{21}^x & \sigma_{22}^x \end{pmatrix} = \varepsilon_x \begin{pmatrix} \beta_x & -\alpha_x \\ -\alpha_x & \gamma_x \end{pmatrix}$$

$$\boldsymbol{\sigma}_z = \begin{pmatrix} \sigma_{11}^z & \sigma_{12}^z \\ \sigma_{21}^z & \sigma_{22}^z \end{pmatrix} = \varepsilon_{x,z} \begin{pmatrix} \beta_z & -\alpha_z \\ -\alpha_z & \gamma_z \end{pmatrix} \quad (3.26)$$

The transformation of the beam matrix from the position s_0 to s can be calculated by

$$\sigma_s = M\sigma_{s_0}M^T, \quad (3.27)$$

where M is the transfer matrix from position s_0 to s.

3.3 FODO structure

In accelerators it is necessary to transport charged particle beams over a long distance without the beam cross-section becoming too large. The simplest arrangement of magnets for this task is the FODO structure (Fig 3.4). It is composed of focusing (F) and defocusing (D) quadrupoles separated by a focusing-free section (O). Since quadrupoles focus only in one plane while defocusing in the other plane, the magnets are arranged one after another with alternating polarity. As a result the FODO system has an overall focusing effect on a beam.

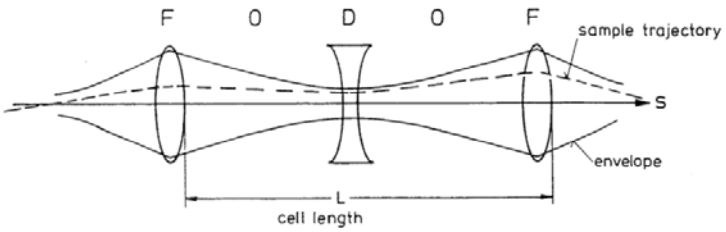

Figure 3.4. FODO structure.

Let us derive the transfer matrices of a FODO structure under the thin lens approximation and assumption that focal lengths are the same for both quadrupoles $f_F = -f_D = f$ and the magnets are separated by a drift space. The horizontal transfer matrix of the FODO cell can be calculated by

$$M_{FODO,x} = M_f M_{drift} M_d M_{drift} M_f \quad (3.28)$$

Where M_f and M_d are the transfer matrices of the focusing and defocusing quadrupoles respectively and M_{drift} is the transfer matrix for drift space.

$$M_{FODO,x} = \begin{pmatrix} 1 - \frac{l^2}{2f^2} & 2l(1 + \frac{l}{2f}) & 0 \\ -\frac{l}{f^2}\left(1 - \frac{L}{2f}\right) & 1 - \frac{l^2}{f^2} & 0 \\ 0 & 0 & 1 \end{pmatrix} \quad (3.29)$$

The transfer matrix of a FODO cell for the vertical plane can be obtained by replacing f by $-f$.

$$M_{FODO,z} = \begin{pmatrix} 1 - \frac{l^2}{2f^2} & 2l(1 - \frac{l}{2f}) & 0 \\ -\frac{l}{f^2}\left(1 + \frac{L}{2f}\right) & 1 - \frac{l^2}{f^2} & 0 \\ 0 & 0 & 1 \end{pmatrix} \quad (3.30)$$

The matrix element M_{21} giving the total focusing/defocusing strength of the system is negative in both cases as long as L<2f, thus providing focusing effect of FODO cell in both planes.

4. Electron Beam Parameter Measurements at AREAL Linac

The lab work consists of two parts. In the (preparatory) PART 1 of the lab work, the students are given an overview of AREAL linac diagnostics, the control system and some background on operation principles. They learn how to work with machine main control tools and to manipulate with electron beam parameters. In the (experimental) PART 2 of the work, the students will perform measurements of the electron beam transverse emittances and beam energy/energy spread. Upon completion of the lab work, students are expected to obtain basic knowledge of electron beam diagnostic methods and hands-on experience in measurement of electron beam main parameters.

4.1. Introduction

Beam diagnostics and instrumentation are an essential part of any accelerator. There is a large variety of parameters to be measured for observation of particle beams with the precision required to tune, operate, and improve the performance of the machine [5].

One of the 1-st questions in the commissioning of a new accelerator is how many particles are in the machine. Thus the beam intensity (bunch current/charge) is one of the most important accelerator parameters. With knowledge of the intensity it is possible to determine lifetime and coasting beam in circular machines, or transfer efficiencies in linacs and transfer lines.

One of the next questions which arise may be where these particles are located, i.e., the position of the beam centroid. Position measurements give access to a wide number of very important accelerator parameters. The most fundamental one is the determination of the beam orbit.

The next question might be how the distribution of particles in space looks, i.e., beam profiles in both transversal and longitudinal dimensions are of interest. Beam size measurements are fundamental for the determination of the beam emittance. Emittance is an important property of charged particle beams, allowing for a description of beam quality and the comparison of beams, as emittance is a constant of motion in many cases.

Another parameter of interest is the beam energy. In synchrotron light sources (third-generation storage rings, as well as free-electron-lasers (FELs)) it defines the spectral characteristics of the emitted radiation. In electron accelerators, the energy distribution of the electron beam is another essential parameter for the study of the longitudinal beam dynamics and beam instabilities.

Currently in the AREAL linac, measurements of electron beam charge, transverse beam shape/size, transverse beam emittances and beam energy/energy spread [6] are foreseen. The schematic layout of the AREAL facility's current state is presented in Fig. 4.1.

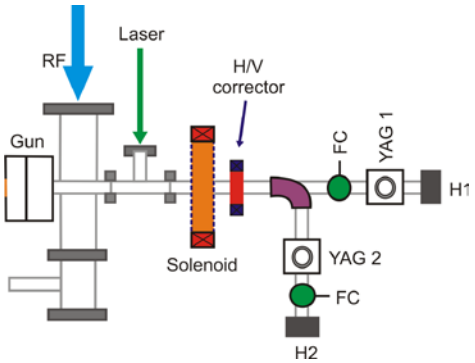

Figure 4.1. Layout of the AREAL electron gun section with diagnostics. Abbreviations are explained in the text.

The current lab work covers measurements of beam energy/energy spread and transverse beam emittances. Both experiments are based on on beam transverse profile measurement.

Beam profile diagnostics are used both for initial tuning of the beam position and beam spot size. A beam spot is the main source of information used to monitor and study the beam transport as well as transverse beam distribution.

The determination of the transverse beam profiles relies on the interaction of beam particles with matter. The method mostly applied is destructive to the beam as it hits a luminescent screen. A part of the deposited energy results in excited electronic states which de-excite partially via light emission. Therefore, the beam profile can be observed via a CCD camera. Sometimes screens are even used as beam position monitors by analyzing the center of gravity of the measured light distribution.

In the AREAL linear accelerator, for beam profile measurements only scintillator crystal (YAG:Ce) based stations are installed. This type of measurement technique is used since for the AREAL electron beam parameters the other possible systems (such as screens based optical transition radiation (OTR) or the wire scanner) would not generate sufficient signal-to-noise ratio.

Two stations are placed in the low energy diagnostic line of the AREAL linear accelerator (Fig. 4.1). Both stations are based on YAG:Ce crystals with 25x25x0.2 mm dimensions. The crystals are mounted to a holder and positioned in the beamline by pneumatic linear motion motors. The scintillators are mounted at the right angle to the beam motion and the emitted light beam repeats the electron beam transverse size in the same direction. The station has two reflecting mirrors. The first mirror is mounted by 45^0 with light direction and reflects the light out of the vacuum chamber. The second mirror is also mounted by 45^0 towards the reflected light from the first mirror and reflects the light by the optical tube to a camera (Fig. 4.2). Since both mirrors are located under 45^0 to the direction of the photon beams, the beam size is not changed during transportation through the projection on mirrors.

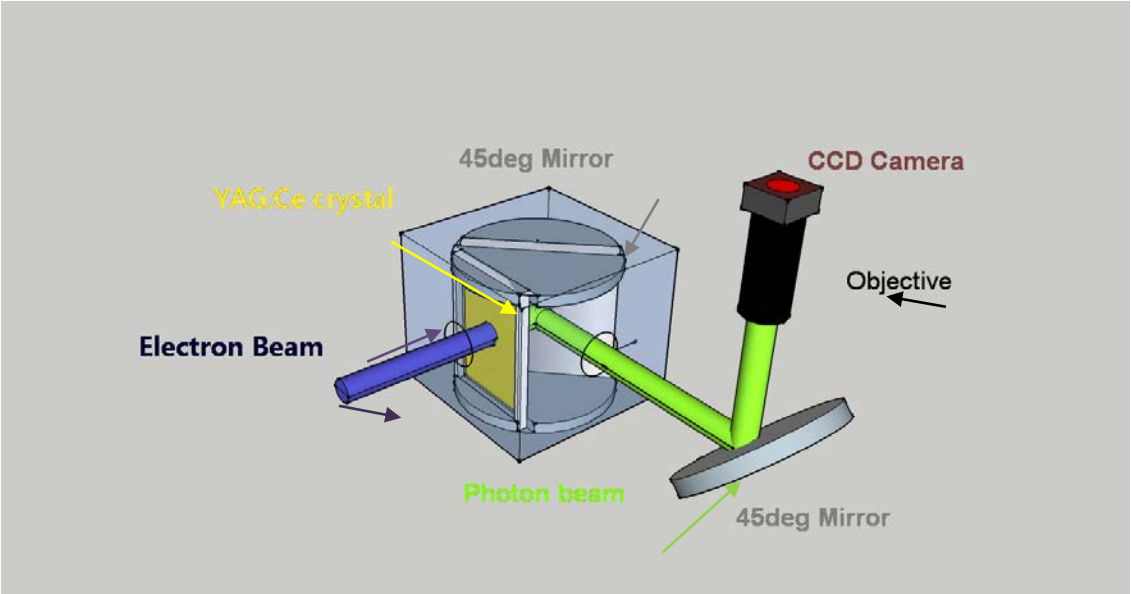

Figure 4.2. Schematic layout of the beam profile measurement

A Point Gray Flea2 08S2 CCD camera at position YAG1 (1032x776 pixels with 4.65 μm size) and a Flea2 20S4 CCD camera (1624x1224 pixels with 4.4 μm size) at YAG 2 stations are used for electron beam transverse profile registration (see Fig. 4.1). The CCD camera signal is transported from the tunnel to the control system via a repeater/HUB. The image is digitized, the beam spot is projected onto orthogonal axes and the statistical properties of the distribution are calculated. The calibration of scales is obtained using reference marks on the screen.

The measurement accuracy of the screen station mainly depends on 3 factors:

- photon beam size deviation from the original electron beam size
- optical system resolution
- data registration and analysis

Photon beam size deviation from the original beam size occurs due to the multiple scattering of the electrons. Passing through a matter, primary electrons are scattered and create secondary electrons and photons, this changes the original direction of their movement. Because of this, the image of the point source will be seen as a distribution with a finite RMS size. As a result, the electron beam image on the CCD camera will be bigger than the real sizes of the beam. YAG crystals at AREAL have 0.2 mm thickness and for 5 MeV beam energy the estimations give 30 μm RMS size of the point electron source.

Another reason of the measurement accuracy degradation is the optical system resolution. At both stations objectives with the same 75 mm focusing lengths of 100 pair/mm resolution are used (5 μm on the photon beam). Later the photon beam is registered by CCD sensors. At YAG1 and YAG2 stations we have 1:7.5 and 1:5 image magnifications, respectively. At YAG1 station 1 pixel corresponds to 34.875 μm beam size and the CCD sensor covers 36x27 mm^2 area of the YAG holder. At YAG2 station the CCD sensor covers 36x26 mm^2 area of the YAG holder and has a 22 μm to 1-pixel transformation.

4.2. Beam energy and energy spread measurements

The measurements of electron beam momentum (energy) and momentum spread (energy spread) are usually done with a magnet spectrometer [5]. The spectrometer transforms the momentum (spread) into a position (spread), as shown in Fig. 4.3, which is measured with a spatial resolving detector (for example YAG screen) according to

$$\frac{\Delta x}{x_0} = \frac{\Delta p}{p_0} . \tag{4.1}$$

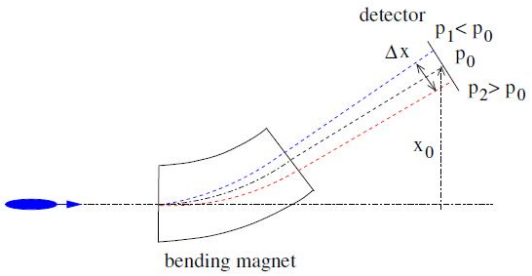

Figure 4.3. Principle of a magnet spectrometer for the momentum (energy) and momentum spread (energy spread) determination.

At the AREAL gun section, a 90° bending magnet is used as a spectrometer. The dipole magnet bends the electron beam, and the beam position is registered by the YAG 2 station. Then the beam momentum *p* (energy) is calculated based on the geometry and calibration of the dipole magnet and the alignment of YAG 2 screen:

$$p = \frac{qlB}{\alpha}, \tag{4.2}$$

where *q* is the electron charge, *B* the magnetic field of the dipole magnet, l is the effective magnetic length and α is the bending angle of the dipole.

The magnetic field of the AREAL spectrometer dipole magnet can be changed from 0 to 200 mT by 0.25 mT steps and has $l = 15.34\,cm$ effective length. Thus the beam momentum (energy) can be determined by

$$p\left[\frac{MeV}{c}\right] = 0.02888\,B[mT]. \tag{4.3}$$

Please verify this relation! The beam energy measurement accuracy depends on magnetic field determination and beam center registration accuracy. Since the determination accuracy of the dipole magnet field is better than 0.25mT, the beam energy measurement accuracy it is about 7.7 keV, which is less than 0.15% for 5 MeV beam energy. The beam registration accuracy at YAG 2 screen is about 50 μm which causes a maximum 0.0625 MeV energy measurement error. This is about 1.25 % for 5 MeV beam energy.

The energy spread is estimated by observing the beam in a dispersive section where the beam horizontal spot size is a convolution of the emittance and dispersion contributions [2]. It can be written to first order as:

$$\sigma_x \approx \sqrt{\beta_x \varepsilon_x + D_x^2 \sigma_E^2}\ , \tag{4.4}$$

where σ_x is the horizontal beam size at the YAG 2 screen located behind the bending at spectrometer arm, ε_x is the horizontal emittance, β_x and D_x are the horizontal beta and dispersion functions and σ_E is the rms energy spread of the beam, respectively. Thus, for the measured energy spread we find:

$$\sigma_E = \frac{\sqrt{\sigma_x^2 - \beta_x \varepsilon_x}}{|D_x|} \leq \frac{\sigma_x}{|D_x|}\ . \tag{4.5}$$

In order to maximize the momentum resolution of the spectrometer, the dispersive contribution to the beam size should be large compared with the emittance contribution ($\beta_x \varepsilon_x \ll D_x^2 \sigma_E^2$). This is achieved by providing horizontal focus (with the help of a solenoid magnet) at YAG 2, thus minimizing β_x.

4.2.1. Electron beam energy and energy spread measurement control tools

For beam energy/energy spread measurements “Dipole_Control” and “Beam_Profile” tools are used. The “Dipole_Control” tool (Fig. 4.4) suggests two options for magnetic field modification: with and without cycling. In the first case the magnetic field is changed taking into account the hysteresis effect.

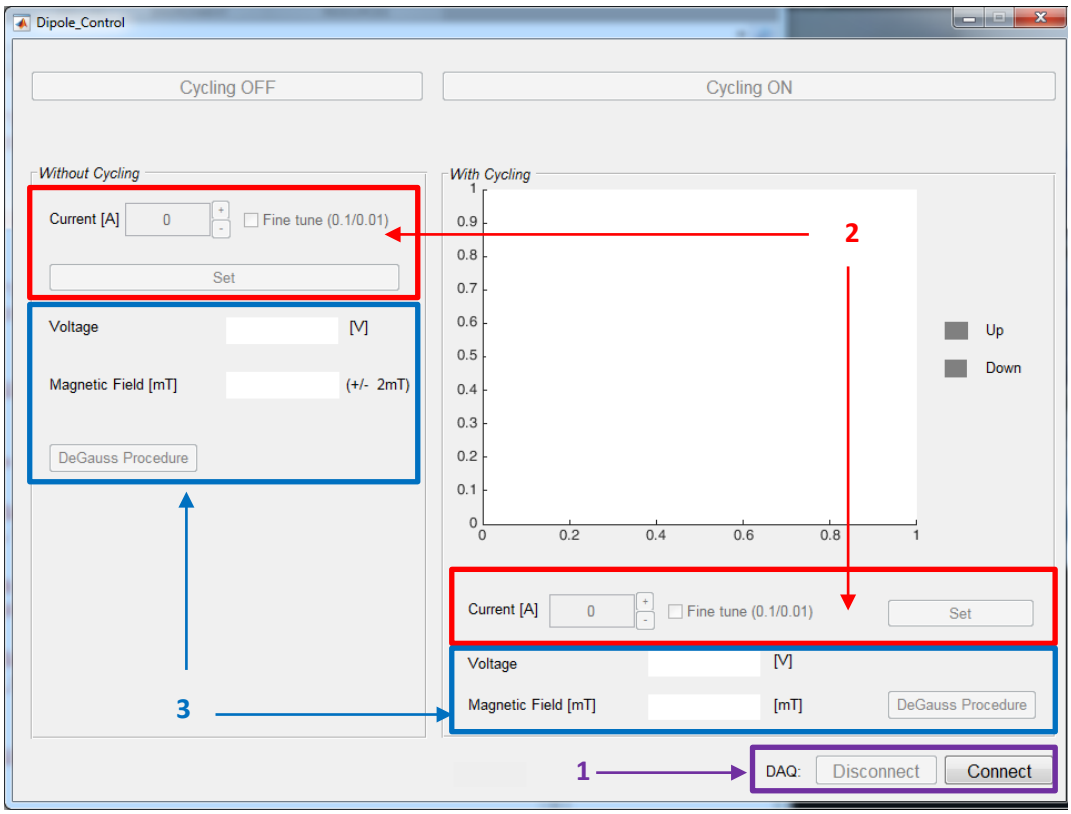

Figure 4.4. “Dipole_Control” tool layout.

The tool consists of the following sections:

Table 4.1. Sections of the Dipole_Control tool.

Section 1: **DAQ**	**Disconnect** - Magnet On **Connect** - Magnet Off
Section 2: **Current**	**Current** - magnet power supply current in A **Set** - set input value for current
Section 3: **Magnet parameters**	**Voltage** - power supply voltage in V **Magnetic Field** - Magnetic field in mT

The interface and sections of the “Beam_Profile” tool are given in Fig. 4.5 and Table 4.2.

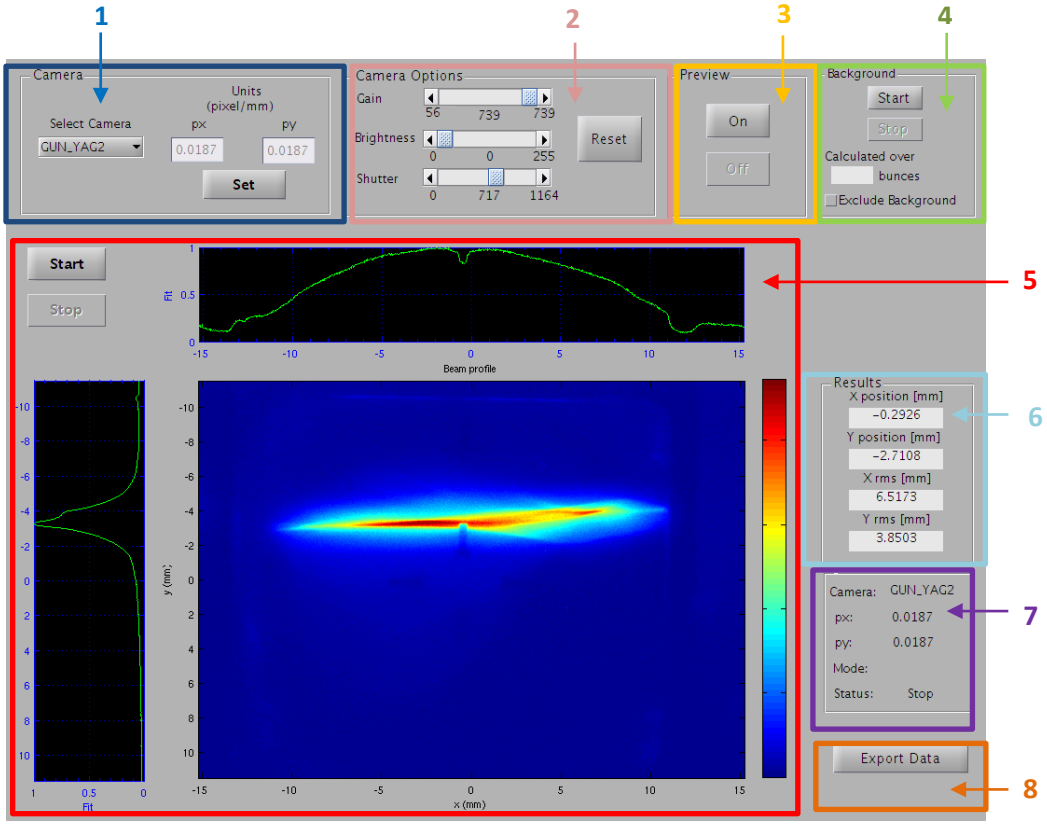

Figure 4.5. Beam_Profile tool layout.

Table 4.2. Sections of the Beam_Profile tool.

Section 1: Camera	**Select Camera** - select camera for beam registration **Units (p_x, p_y)** - camera pixel to mm interpretation coefficients **Set** - click to set coefficients
Section 2: Camera Option	**Gain** - camera gain value **Brightness** - camera brightness value **Shutter** - camera shutter value
Section 3: Preview	**On** - switch on camera on preview mode **Off** - switch off camera
Section 4: Background	**Start** - start background data scan **Stop** - stop background data scan **Calculated over** - background data calculation period **Exclude background** - select to exclude background in Section 5 view and calculation of results in Section 6
Section 5: Beam profile	**Start** - start beam registration and data analysis **Stop** - stop beam registration and data analysis **Beam Profile** - registered beam transverse profile **Fit** - horizontal/vertical fit of the beam intensity
Section 6: Results	**X position** - horizontal position of the beam center

	Y position - vertical position of the beam center **X rms** - horizontal rms size of the beam profile **Y rms** - vertical rms size of the beam profile
Section 7: Camera parameters	**Camera** - selected camera name **px/py** - camera pixel to mm interpretation coefficients **Mode** - show camera run mode **Status** - camera status (start/stop)
Section 8: Export data	**Export data** - click to save data

For the beam energy spread measurement, a quadrupole magnet is used to additionally focus the electron beam on YAG 2 screen. The layout of the quadrupole magnet control tool “Quadrupole_PS” and its sections are given below:

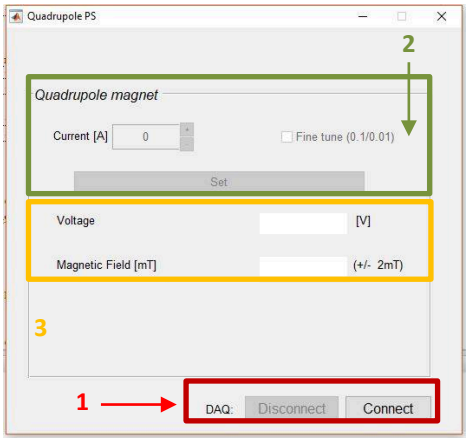

Figure 4.6. Quadrupole_PS tool layout

Table 4.3: Sections of the Quadrupole_PS tool.

Section 1: **DAQ**	**Disconnect** - Magnet On **Connect** - Magnet Off
Section 2: **Current**	**Current** - magnet power supply current in A **Set** - set input value for current
Section 3: **Magnet parameters**	**Voltage** - power supply voltage in V **Magnetic Field** - Magnetic field in mT

4.2.2. Measurement tasks

- Measure the beam energy

- Change the magnetic field of the dipole until the beam is observed at YAG 2 screen.
- Fine tune the position (dipole field) of the beam center such that it coincides with the YAG 2 crystal center.
- Calculate the beam energy with formula (4.3).

- Estimate the beam energy spread
  - After completing the first two steps of the previous task, achieve maximum horizontal focusing on YAG 2 screen by adjusting the field of the quadrupole magnet.
  - Measure the beam spot size by using the “Beam_Profile” control tool.
  - Estimate the beam energy spread using formula (4.5) ($D_x = 0.2401\ m$).

4.2.3 Measurement procedure

At the AREAL linac the electron beam energy is measured by the following procedure:

1. Run “Dipole_Control” tool and press Connect button at the Section 1 (Fig. 4.4).
2. Start “Beam Profile” tool and select camera Gun_YAG2 at the “Select Camera” field in Section 1 (Fig. 4.5).
3. Push “On” button in Section 3 to register electron beam (Fig. 4.5).
4. Tune the magnet field until the beam is observed by changing the current value in “Current” field of Section 2 (Fig. 4.4).
5. After the beam observation, switch off the preview mode in Section 3, start the background scan by pushing the “Start” button in Section 4, then check “Exclude Background” (Fig. 4.5).
6. Start the beam observation and data analysis by pressing the “Start” button in Section 5 (Fig. 4.5).
7. Tune the value of the magnet current to move the electron beam to the center of the screen.
8. Fix the current value and determine the beam energy from the calibration curve given in Fig. 4.7.

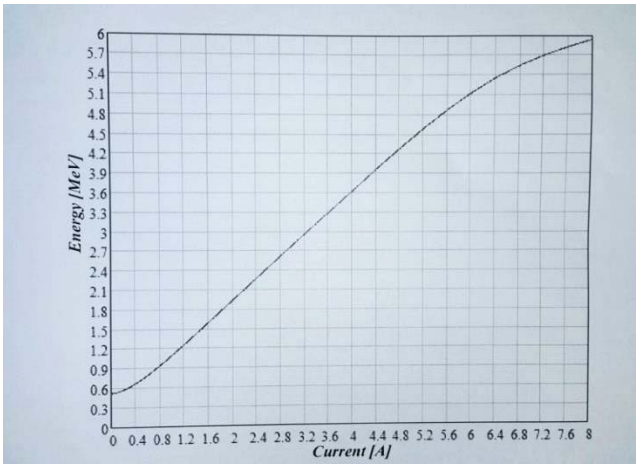

Figure 4.7. Dipole magnet current vs electron beam energy at AREAL. The students should discuss, why this curve is not perfectly linear !

In order to estimate the beam energy spread the following steps should be performed:

1. Start the "Quadrupole_PS" tool after the beam energy measurement procedure (8 steps described above).
2. Switch on the quadrupole magnet by pushing the "Connect" button in Section 1 (Fig.4.6).
3. Change the current value at the "Current" field of Section 2 to change the quadrupole strength (Fig. 4.6) until the maximum horizontal focusing at the YAG2 station is reached (Fig. 4.5).
4. Estimate the beam energy spread using formula (4.5).

4.3. Beam Transverse Emittance Measurements

Emittance is an important property of charged particle beams, allowing for a description of beam quality and the comparison of beams. One of the most challenging directions in electron beam physics and accelerator technologies is the generation of high brightness powerful shortwave electromagnetic radiation. To generate high brightness powerful radiation, it is mandatory to produce charged particle beams with low emittance and high energy. The brightness is defined as

$$B = \frac{F}{4\pi^2 \varepsilon_x \varepsilon_z}, \tag{4.6}$$

where *F* is the photon flux, defined as the number of radiated photons per second and within spectral bandwidth of 0.1%, ε_x and ε_z are the horizontal and vertical emittances, respectively.

There are different techniques for measuring the transverse beam emittance [7]. In this course the Solenoid/Quadrupole scan technique will be considered.

4.3.1. Solenoid/Quadrupole scan technique

A solenoid is a tightly wound helical coil of wire (Fig. 4.8, a). The magnetic field generated in the core, of a current carrying solenoid is essentially uniform, and is directed along the axis of the solenoid. Outside the solenoid, the magnetic field is far weaker. This magnet is often used to focus charged particle beams in the low energy section of accelerators and other devices such as electron microscopes. The quadrupole magnet (Fig. 4.8, c) consists of four iron pole shoes with hyperbolic contour.

Solenoid and quadrupole scan techniques have the same underlying principle, which is to measure the beam size of the particle beam as a function of the magnetic field strength of a solenoid/quadrupole magnet at a beam size detector (for example YAG screen). If the transformation matrix of the whole path of beam transportation is known, the beam matrix components can be defined and hence the emittance can be calculated. Alternatively, it is possible to measure the beam size at different positions without any additional change of the magnetic fields. At AREAL the first method is used.

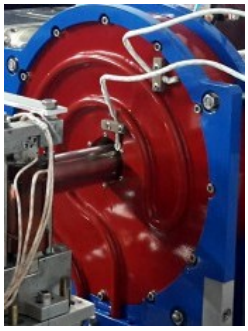

a)

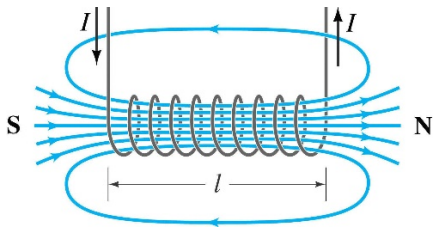

b)

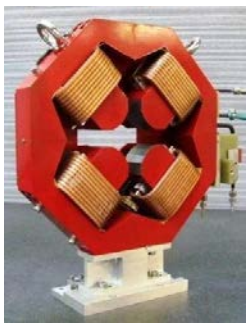

c)

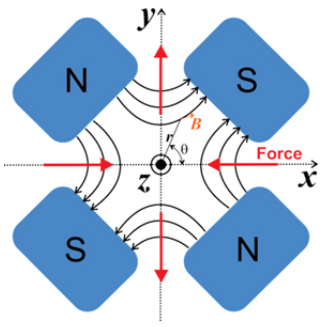

d)

Figure 4.8. a, b) solenoid magnet; c,d) quadrupole magnet

Let *R* be the total transformation matrix for the solenoid/quadrupole and drift spaces from distance s to s_0:

$$R = \begin{bmatrix} R_{11} & R_{12} \\ R_{12} & R_{22} \end{bmatrix}. \tag{4.7}$$

Recall (see Eq. (3.27)) that the beam matrix at position s is related to beam matrix at s_0 by

$$\sigma(s) = R(s)\sigma(s_0)R^T(s). \tag{4.8}$$

The first term in the resultant matrix is

$$\sigma_{11}(s) = \sigma_{11}(s_0)R_{11}^2 + 2\sigma_{12}(s_0)R_{11}R_{12} + \sigma_{22}(s_0)R_{12}^2. \tag{4.9}$$

If *Q* represents the transfer matrix of the solenoid/quadrupole and *S* represents the transfer matrix between the solenoid/quadrupole and the imaging screen (Fig. 4.9), then in the thin lens approximation the transfer matrices may be written as:

$$R = \begin{bmatrix} S_{11} + KS_{12} & S_{12} \\ S_{21} + KS_{22} & S_{22} \end{bmatrix}, \tag{4.10}$$

where (see Eq. (2.35))

$$Q = \begin{bmatrix} 1 & 0 \\ K & 1 \end{bmatrix}, \quad S = \begin{bmatrix} S_{11} & S_{12} \\ S_{21} & S_{22} \end{bmatrix} \tag{4.11}$$

(K is the integrated field strength 1/f of the solenoid/quadrupole magnet).

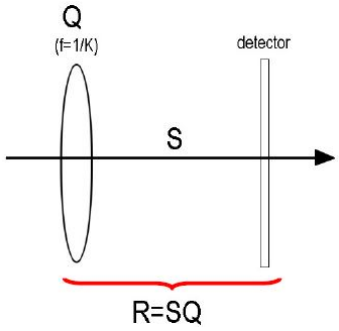

Figure 4.9. The schematic layout of the setup.

Thus, eq. (4.9) takes the form

$$\sigma_{11}(s) = (S_{11} + KS_{12})^2\sigma_{11}(s_0) + 2S_{12}(S_{11} + KS_{12})\sigma_{12}(s_0) + S_{12}^2\sigma_{22}(s_0), \tag{4.12}$$

or

$$\sigma_{11}(s) = AK^2 + BK + C \tag{4.13}$$

where

$$A = S_{12}^2 \sigma_{11}(s_0),$$

$$B = 2S_{11}S_{12}\sigma_{11}(s_0) + 2S_{12}^2\sigma_{12}(s_0), \tag{4.14}$$

$$C = S_{11}^2 \sigma_{11}(s_0) + 2S_{11}S_{12}\sigma_{12}(s_0) + S_{12}^2\sigma_{22}(s_0).$$

Acquiring a set of beam size measurements at detector location s as the solenoid/ quadrupole field strength is scanned over a range of values (around the value providing maximal focused beam), and using least squares for parabolic fitting, A, B, C parameters can be determined. Then beam matrix elements at location s_0 can be found from (4.14), allowing to calculate the emittance with (3.20).

4.3.2. Emittance determination errors1

Let $\vec{x} = \{x_1, x_2, \dots x_n\}^T$ be n random variables with known covariance matrix V(x). Let $\vec{y} = \{y_1, y_2, \dots y_n\}^T$ with $y_j = y_j(x_1, x_2, \dots x_n)$, are variables dependent on $\vec{x}$. Then the covariance matrix V(y) is given by [8]

$$V(y) = B \cdot V(x) \cdot B^T \tag{4.15}$$

where the matrix B is the Jacobian defined as:

$$B = \begin{pmatrix} \frac{\partial y_1}{\partial x_1}\frac{\partial y_1}{\partial x_2} & \cdots & \frac{\partial y_1}{\partial x_n} \\ \frac{\partial y_2}{\partial x_{12}}\frac{\partial y_2}{\partial x_2} & \cdots & \frac{\partial y_2}{\partial x_n} \\ \vdots & & \\ \frac{\partial y_m}{\partial x_1}\frac{\partial y_m}{\partial x_2} & \cdots & \frac{\partial y_m}{\partial x_n} \end{pmatrix} \tag{4.16}$$

In the special case of a linear transformation $\vec{y} = B_1 \cdot \vec{x}$, the Jacobian *B* is simply the matrix B_1, which defines the linear transformation.

Now, considering (4.9), the entire measurement can be written in a vector form as follows

$$\underbrace{\begin{pmatrix} \sigma_{11}^{(1)}(s) \\ \sigma_{11}^{(2)}(s) \\ \vdots \\ \sigma_{11}^{(n)}(s) \end{pmatrix}}_{\vec{b}} = \underbrace{\begin{pmatrix} R_{11}^{(1)2} & 2R_{11}^{(1)}R_{12}^{(1)} & R_{12}^{(1)2} \\ R_{11}^{(2)2} & 2R_{11}^{(2)}R_{12}^{(2)} & R_{12}^{(2)2} \\ \vdots & & \\ R_{11}^{(n)2} & 2R_{11}^{(n)}R_{12}^{(n)} & R_{12}^{(n)2} \end{pmatrix}}_{M} \cdot \underbrace{\begin{pmatrix} \sigma_{11}(s_0) \\ \sigma_{12}(s_0) \\ \sigma_{22}(s_0) \end{pmatrix}}_{\vec{a}} \tag{4.17}$$

[1] This section is merely a practical reference how to estimate errors of emittance and can not replace the standard statistics lectures.

where the index *n* in brackets indicates the number of performed measurements. The solution of (possibly over determined) system of equations (4.14) is given by the so-called normal equation

$$\vec{a} = \underbrace{(M^T \cdot M)^{-1} \cdot M^T}_{B} \cdot \vec{b} \tag{4.18}$$

In the following only the error δΣ of the r.m.s. beam size measurement is going to be considered. It is important to note that the elements of the vector $\vec{b}$ in eq. 4.18 are the squared beam sizes ($\Sigma^2 = \sigma_{11}$). If one for example assumes a constant fractional error of $\delta\Sigma/\Sigma = \eta$ (e.g. $\eta = 5\ \%$), then the error of the squared beam size $\delta\Sigma^2 \approx 2\Sigma\delta\Sigma = 2\eta\Sigma^2$. Since the individual measurements are independent from each other, the covariance matrix of the squared beam sizes has a diagonal form

$$V(b) = diag[var(\Sigma_1^2),\ var(\Sigma_2^2), \dots ,\ var(\Sigma_n^2)] =$$

$$= diag[4\eta^2\Sigma_1^4,\ 4\eta^2\Sigma_2^4,\ \dots, 4\eta^2\Sigma_n^4] \tag{4.19}$$

The procedure of the error estimation consists of two steps or two error propagations respectively. In the first step the covariance matrix V(a) of the statistical quantities a_i is obtained straightforward from eq. (4.15) with the matrix B as defined in eq. (4.18)

$$V(a) = [(M^T \cdot M)^{-1} \cdot M^T] \cdot V(b) \cdot [(M^T \cdot M)^{-1} \cdot M^T]^T. \tag{4.20}$$

Remember that the matrix M is known from the calibration of the quadrupole and the known geometry of the measurement set-up (see eq. (4.7), (4.10), (4.17)).

In the next step, again using eq. (4.15), one obtains the variance

$$var(\varepsilon_x) = J \cdot V(a) \cdot J^T, \tag{4.21}$$

where $J = \left(\frac{\partial\varepsilon_x}{\partial a_1}, \frac{\partial\varepsilon_x}{\partial a_2}, \frac{\partial\varepsilon_x}{\partial a_3}\right)$ (see eq. (3.20) and (4.17)).

4.3.3. Emittance measurement tool

For the electron beam emittance measurement at AREAL linac, the EMIT tool is used. The tool consists of eight main sections which are presented in Fig. 4.10. The tool sections are described in Table 4.4.

Table 4.4. Description of EMIT tool.

Section 1: Camera selection	**Cam1**-*Camera of the YAG1 station* **Cam2**- *Camera of the YAG2 station*
Section 2: Magnet selection	**QF**- *Quadrupole magnet* **Sol** - *Solenoid magnet*
Section 3: Beam image and sizes	*Beam transverse spot image (intensity map) with projections into horizontal and vertical axes*
Section 4: Beam parameters	$\boldsymbol{\sigma_x}$ *– horizontal size* $\boldsymbol{\sigma_y}$ *– vertical size* **x position** *– horizontal offset of the registered beam center* **y position** *– vertical offset of the registered beam center*
Section 5: Scan parameters	**Emittance orientation** *– choose measured emittance* $(\varepsilon_x/\varepsilon_y)$ **Initial value** *– magnet initial field value for measurement* **Step size**- *magnet field changing size* **Step count** – number *of measurements* **Data per measurement**- *number of measurements in one step*
Section 6: Start/Cancel buttons	**Start -** *start emittance measurement* **Cancel –** *stop emittance measurement*
Section 7: Fit window	**Equation –** *quadratic equation of the fit curve* **Save result –** *save measurement data and calculation results*
Section 8: Results	$\boldsymbol{\sigma_{11}, \sigma_{22}, \sigma_{33}}$ **–** *elements of the beam matrix* $\boldsymbol{\varepsilon_x/\varepsilon_y}$ **–** *value of the measured emittance*

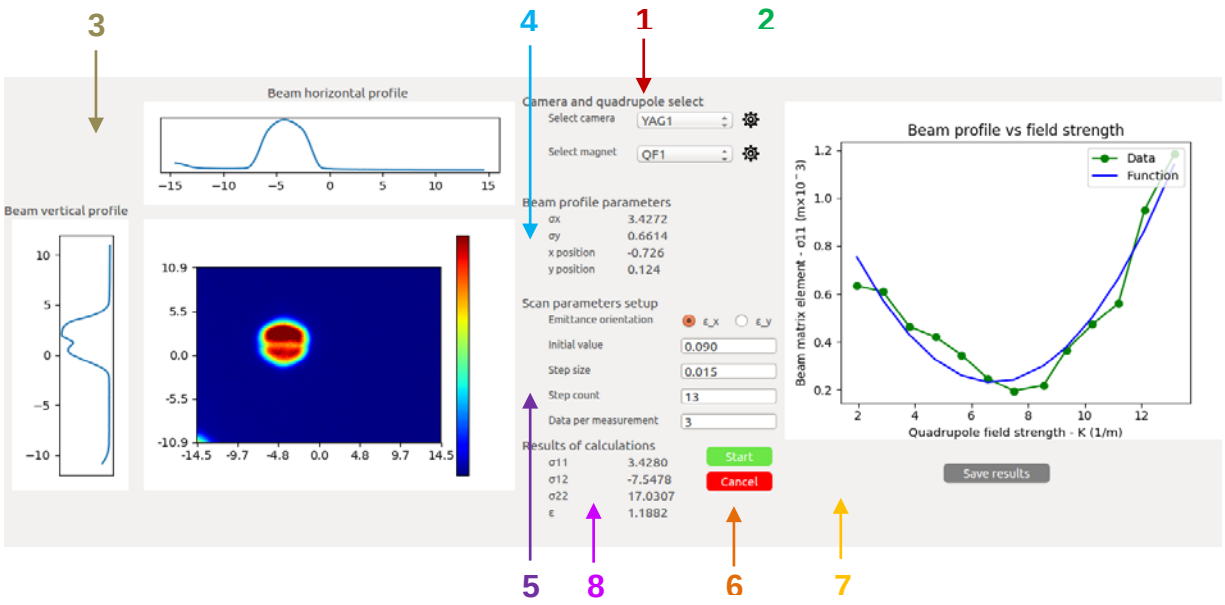

Figure 4.10. EMIT tool interface.

4.3.4. Measurement tasks

Measure transverse beam emittance using solenoid/quadrupole scan method.

- Deliver electron beam to YAG 1 screen.
- Obtain a minimum spot size (maximum focused beam) changing the quadrupole field.
- Acquire a set of beam size measurements around the maximum focusing point.
- Calculate A, B, C parameters using least squares method for parabolic fitting.
- Calculate the beam emittance using formulae (3.20) and (4.14).

4.3.5. Measurement procedure

The measurement procedure of the transverse beam emittance at the AREAL linac (using quadrupole scan method) is the following:

1. Run the EMIT tool
2. Select Cam1 in Section 1 for beam registration at the YAG1 station
3. Observe the electron beam delivered to the YAG 1 screen in Section 3
4. Select the QF quadrupole magnet in Section 2.
5. Use 0 as initial value for the quadrupole magnetic field, 0.02 step size and 20 steps in Section 5.

6. Push Start button in Section 6 to start measurements.
7. Find the magnet field value for minimum spot size (maximum focused beam) from the green curve in Section 7.

- Return to Step 5 if the minimum spot size is not reached and use more steps (for example 40).

8. Use a better initial value of the magnetic field (the initial value must be chosen so that the beam size measurements are made around the maximum focusing point), smaller step size (< 0.015), more than 10 steps for better fit of measurement data and push Start button in Section 6.
    - In order, to minimize influence of the beam fluctuations during the measurements, more than one beam can be registered for one field value (**Data per measurement,** Section 5). Afterwards, the average of these measurements will be considered as a beam size in this point.
9. Push **Save results** button in Section 7 to save the calculated emittance value and measurement data in a local file.
10. Estimate emittance calculation error by assuming 5% constant fractional error of $\delta\Sigma/\Sigma$.

Bibliography

1. *K.* Wille, *Physics of Particle* Accelerators, Oxford University Press, 2001.
2. P. Schmüser, J. Rossbach, *Basic Course on Accelerator Optics*, In CAS-CERN Accelerator School: 5th General Accelerator Physics Course, 1993.
3. Ph. Royer, *Solenoidal Optics*, PS/HP Note 99-12, Neutrino Factory Note 11, 1999.
4. H. Wiedemann, *Particle Accelerator Physics*, Springer, 3ed., 2007.
5. G. Kube, CERN–2009–005, pp. 1-64.
6. A. A. Sargsyan et al., Journal of Instrumentation, T03004, 2017.
7. K. T. McDonald, D. P. Russell, Frontiers of Particle Beams; Observation, Diagnosis and Correction. Lecture Notes in Physics, v. 343. Springer, 1989.
8. E. Blobel, E. Lohrmann, Statistische und numerische Methoden der Datenanalyse. Wiesbaden: Teubner, 1998, ISBN 978-3-935702-66-9, (see Sec 4.9) http://www-ibrary.desy.de/elbook.html